World Academy of Science, Engineering and Technology
International Journal of Chemical and Materials Engineering
Vol:18, No:7, 2024

Friction Behavior of Wood-Plastic Composites against Uncoated Cemented Carbide

A. Vilutis, V. Jankauskas

***Abstract*—**The paper presents the results of the investigation of the dry sliding friction of wood-plastic composites (WPCs) against tungsten carbide-cobalt (WC-Co) hard alloy. The dependence of the dynamic coefficient of friction on the main influencing factors (vertical load, temperature, and sliding distance) was investigated by evaluating their mutual interaction. Multiple regression analysis showed a high polynomial dependence (adjusted $R^2 > 0.98$). The resistance of the composite to thermo-mechanical effects determines how temperature and force factors affect the magnitude of the coefficient of friction. WPC-B composite has the lowest friction and highest resistance compared to WPC-A, while composite and cemented carbide materials wear the least. Energy Dispersive Spectroscopy (EDS), based on elemental composition, provided important insights into the friction process.

***Keywords*—**Friction, composite, carbide, temperature.

I. Introduction

FRICTION is the force of resistance to movement, and while it can be very useful, it also has negative effects. Tribological contacts consume approximately 23% (119 EJ) of the total global energy, with friction losses accounting for 20%. In the long term (15 years), the use of new surfaces, materials and lubrication technologies can reduce energy losses due to friction and wear in vehicles, machines and other equipment by 40% [1].

For plastics and polymer composites to successfully replace metallic materials, a good knowledge of the materials themselves (structure, manufacture and processing, viscoelastic behavior, etc.) [2] and tribological parameters (friction, wear, contact temperature, etc.) is necessary in order to be able to make right decisions [3]. WPCs are gaining popularity due to their inherent benefits and increasing global environmental issues, with annual consumption reaching 7 million tons by 2025 [4] and demand increasing by 11.5% between 2022 and 2030 [5]. Most of them are made by extrusion, the rest by injection molding, compression molding and other processes [6]. A large selection of extrusion lines is available (with one or two co-rotating or counter-rotating screws, etc.) [7]. The coefficient of friction is an important indicator for optimizing manufacturing energy efficiency and WPC functional properties [8]. The coefficient of friction is exponentially dependent on the pressure in the mixing chamber along the screw [9] and must be optimal for various processes (compression, melting, transportation, etc.) [6], [9], [10]. Depending on the diameter and rotation speed of the extruder screws, materials slide at speeds from a few tenths to several $m \cdot s^{-1}$ [11], while the speed of mechanical processing reaches several tens of $m \cdot s^{-1}$. Tools wear out intensively due to friction and abrasive wear [12], [13]. During the secondary production process, WPC shows different behavior, some of the reasons are unknown and more detailed investigations are needed [14].

The aim of this research was to investigate the dry friction process of two different WPCs against WC-Co hard alloy and to determine the essential dependencies.

II. Materials and Methods

A. Materials

Two types of solid extruded WPCs were purchased on the local market and used for the research: 1) alternatively designated WPC-A, made from hard unplasticized (rigid) amorphous recycled thermoplastic polyvinyl chloride (PVC-U) and the Scots pine (*Pinus sylvestris*); 2) WPC-B, from the primary processing of a semi-crystalline high-density polyethylene (HDPE) and Moso bamboo (*Phyllostachys pubescens*). WPC-A is a composite of 50% plastic, 45% wood particles and 5% additives while WPC-B consists of 60% wood particles, 30% plastic and 10% additives (by weight). The boards were machined into the smooth (Ra ≈ 1.6 μm) wheels of the composites under study. When testing under different experimental conditions, the terms WPC-B1 and WPC-B2 were introduced.

Carbide inserts T04MG-CR were manufactured by Tigra GmbH. The dimensions are shown in Fig. 1.

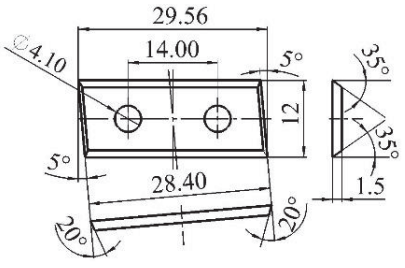

Fig. 1 Uncoated WC–Co carbide blade drawing

The blade consists of tungsten carbide (WC) – 95.2% (grain size 0.7-1.0 μm), binder cobalt (Co) – 4.3%, also nickel (Ni) and chromium (Cr). The main cutting edge and the grinding direction are at an angle of about 10° degrees.

A. Vilutis and V. Jankauskas are with the Department of Mechanical, Energy and Biotechnology Engineering, Vytautas Magnus University, K. Donelaičio str. 58, LT-44248 Kaunas, Lithuania (phone: +37060446435; e-mail: almontas.vilutis@vdu.lt, vytenis.jankauskas@vdu.lt).

B. Characterization of the Samples

1) Mechanical Characterization

The main technical data of the carbide inserts were provided by the manufacturer and presented in Table I.

TABLE I
THE MAIN PROPERTIES OF THE UNCOATED WC-CO [15]

Property	Units	Value
Density	$kg \cdot m^{-3}$	15050
Hardness	HV10	1900
Young's modulus	GPa	645
Flexural strength	GPa	2.35
Poisson's ratio	unitless	0.22
Fracture toughness	$MPa \cdot m^{0.5}$	8.6
Thermal conductivity	$W/(m \cdot K)$	90
Thermal expansion	$x10^{-6} K^{-1}$	4.5

The main properties of the composite materials (density, hardness, strength) were determined in a laboratory of Vytautas Magnus University. Density was determined by weighing samples of known dimensions d12.75xL25.4 mm and then performing analytical volume and density calculations. Hardness was determined by pressing a 6 mm alumina ceramic ball with a T211 pressing device. Requirements of the standards ASTM E10-14/ASTM E103 were followed for hardness testing. The preload was 10 kgf and the test force of 100 kgf was set within 10 s and held for 15 s. The resulting Brinell HBN hardness values were converted to MPa units. Tensile and compression tests were performed with an Instron 5965 universal testing machine, the test speed was 20 $mm \cdot min^{-1}$ (tolerance ± 10%). The dimensions of the samples are shown in Fig. 2. Samples were made and tested both along and across the direction of extrusion. ASTM D638-14 standard was followed for the tensile testing and ASTM D695 was used for compression testing. One end of the tensile samples was fixed. The ambient temperature during the tests was 21 ± 1 °C and the relative humidity was 40%. The average data of 3 replicates are presented. Strength and modulus values were calculated analytically from the stress-strain curves obtained.

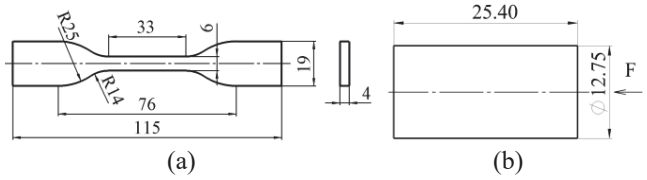

Fig. 2 Dimensions of the specimens for the test of mechanical properties: (a) tensile; (b) compression

2) Morphology Characterization, Profile Roughness and Weight

Before conducting the tribological test, the surface of the milled composites was examined using and Inskam315 LCD digital microscope (DM). The biggest particle size (length and width of 100 randomly selected wood particles of each species) was estimated. The WC-Co surface was examined using a Hitachi S-3400N SEM and a Bruker AXS Quad 5040 EDS analyzer (the central part of the most worn areas was examined and EDS data are presented as the average of two measurements). Profile roughness parameters (Ra, Rsm, Rp and Rdq) were measured using a MahrSurf GD25 profilometer with a 2 μm needle. Roughness was evaluated perpendicular to the direction of rotation of the wheel both before and after the test. All samples were weighed with a Kern ABJ 320-4NM analytical balance (0.1 mg accuracy).

C. Methods

Friction tests with a tribometer SMC-2 were carried out using the rotating disc (WPC)–flat plate (WC-Co) scheme which is shown in Fig. 3. Fig. 4 shows the load diagram.

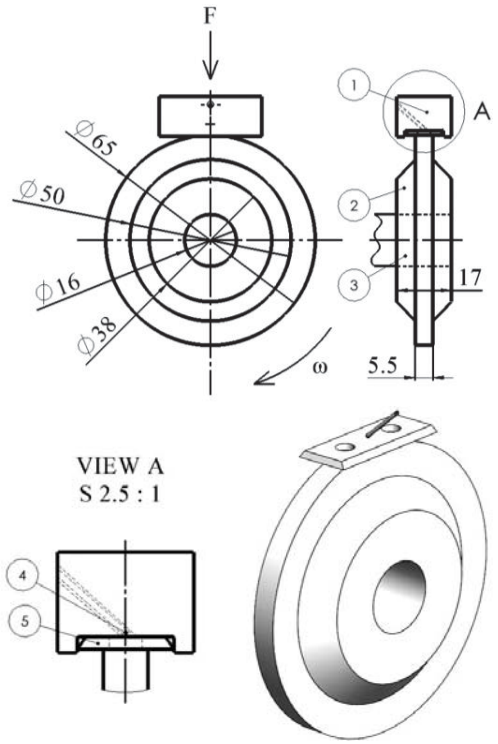

Fig. 3 Test scheme: 1-metal holder; 2-wheel of the material under study; 3-shaft; 4-K-type thermocouple (at a distance of ≈1.5 mm from the contact center); 5–cemented carbide plate

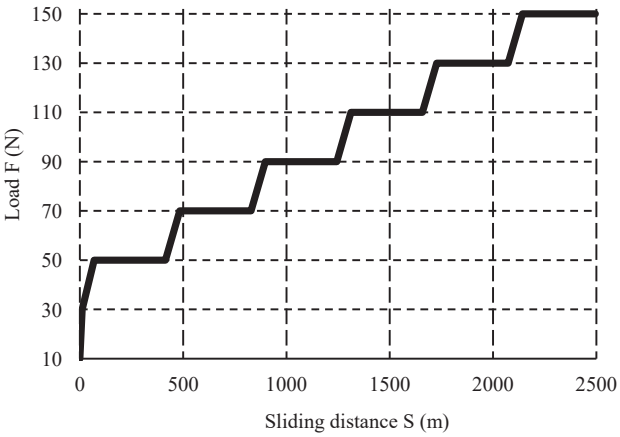

Fig. 4 Load diagram

The software control is activated after the preload of 10 N has been set on the tribometer. As the composite sample begins to rotate, the load is increased to 30 N in 10 s and to 50 N in 1 min. After that, the test mode is constant, the load is held for 5 min and increased by 20 N in 1 min (stepped load cycles). The speed of the shaft was not changed and was 338.8 rpm. The temperature was recorded at 300 ms intervals while the other data were recorded at 4 ms intervals. The total time was ≈36 min. or ≈2.5 km of sliding distance (≈12.25 thousand revolutions) and the linear sliding speed was 1.15 m·s^{-1}. As there was no significant plastic degradation observed of the composite WPC-B wheels, the test was extended until ≈51 min.

D. Data Analysis

According to the data obtained, multiple regression analysis was performed [16], [17], and the interaction of the studied factors was evaluated according to (1):

$$\mu = \beta_0 + \beta_1 S + \beta_2 F + \beta_3 T + \beta_4 SF + \beta_5 ST + \beta_6 FT + \\ + \beta_7 FST + \varepsilon. \quad (1)$$

where: μ - variable (dynamic coefficient of friction); β_i (i = 0,1, …7) - regression coefficients; S, F, T - independent variables (S - sliding distance, m; F-normal force, N; T - temperature, °C); ε - residual error.

During analysis of variance (ANOVA), the significance of the regression model was assessed according to the Fisher's F-test criterion, testing the hypotheses (level of significance $\alpha = 0.05$): H_0: $\beta_i = 0$, i = 1,2, ..., n; H_1: at least one coefficient β_i is non-zero. Only the coefficients with $p < 0.05$ were included in the model.

The mass loss of composites and the hard alloy was evaluated according to (2):

$$W_l = m_0 - m_1. \quad (2)$$

where: W_l - mass loss, mg; m_0 - mass of the sample before testing, mg; m_1 -mass after test, mg.

The value of the sample mean was estimated with a 95% confidence interval CI:

$$CI = \bar{x} \pm 1.96 \cdot SE. \quad (3)$$

where: CI - confidence interval, $\bar{x}$ - sample mean, SE - sample mean standard error.

Data were processed with the programs MS Excel, MATLAB R2023a and Gwyddion 2.61.

III. Results and Discussion

A. Mechanical test Results

The main mechanical properties of WPCs are presented in Table II. As can be seen, density and hardness are quite similar and both WPCs demonstrate almost isotropic behavior in compression. Meanwhile, tensile strength in the direction of extrusion is several or more times higher than in the transverse direction. Shear strength also varies in different directions, as does fracture toughness, although these are not presented here. Extruded WPCs can be modeled as transversely isotropic composites. However, the focus of this study has not been to fully describe the mechanical properties of the extruded WPCs.

TABLE II
The Main Properties of WPCs

Property	WPC-A	WPC-B
Density, kg·m^{-3}	1380	1324
Hardness, MPa	181.88	158.61
Compressive modulus E_c, GPa	1.62	1.60
Tensile strength ∥[a], MPa	33.20	20.46
Tensile strength ⊥[b], MPa	5.61	12.10
Compressive strength ∥, MPa	32.70	25.51
Compressive strength ⊥, MPa	32.71	24.44

[a]∥-longitudinally and [b]⊥-transversely to the direction of extrusion

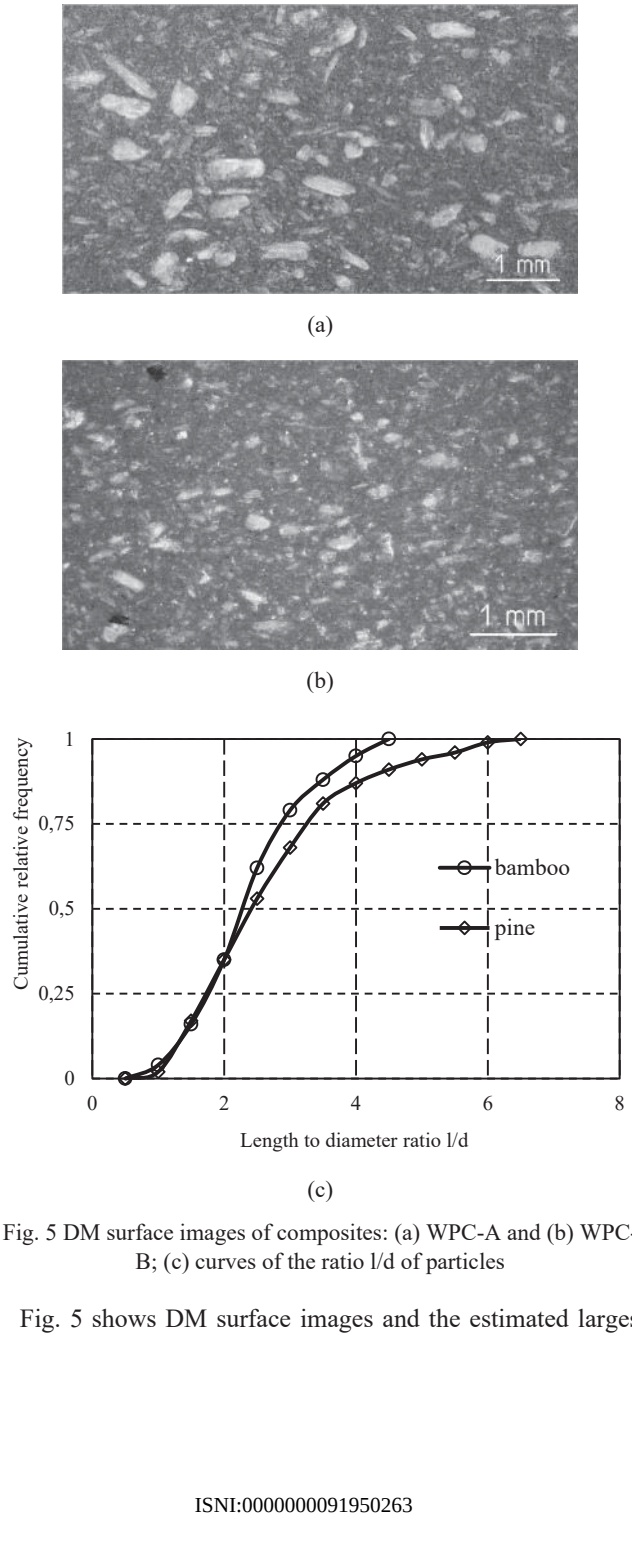

Fig. 5 DM surface images of composites: (a) WPC-A and (b) WPC-B; (c) curves of the ratio l/d of particles

Fig. 5 shows DM surface images and the estimated largest

particle size of WPCs.

Bamboo particles have an average length of l = 0.31 ± 0.02 mm and a diameter of d = 0.11 ± 0.007. The average size and scatter of pine wood particles is larger: l = 0.47 ± 0.04 mm, d = 0.16 ± 0.01 mm. Bamboo particles have a narrower l/d ratio range and more consistent diameters, which can result in more even load transfer from thermoplastic to wood, more even yield stress distribution, and improved interfacial adhesion. More extensive investigations into WPC properties and compositions require additional research.

B. Friction Test Results

The average curves of the evolution of the dynamic coefficient of friction (COF) are shown in Fig. 6. In all cases, the WPC-A composite wheels did not withstand the thermomechanical loading, but WPC-B did, which is why a more detailed designation was introduced: those that withstood the loading were designated WPC-B1, those that did not withstand due to significant plastic deformation, as WPC-B2.

The coefficient of friction μ is given from a normal force of 30 N. During the running-in phase, it increases rapidly until the first constant load of 50 N is reached. For the WPC-A composite, the coefficient of friction increases gradually from 0.11 to 0.12 as the load increases from 50 to 130 N, and such a steady increase is present in each constant load interval. Only after reaching a temperature of ≈ 82 °C, μ suddenly begins to increase until it reaches a maximum value of 0.203. Meanwhile, WPC-B1 exhibits a more pronounced variation. Up to 110 N, the load increases exponentially and after 5 min of maintaining the applied load it changes linearly in each interval. When the load is increased from 110 to 170 N, it decreases, but in each loading interval a linear upward trend is observed. After extending the test time with the WPC-B2 composite and further increasing the load from 170 to 210 N, the material can no longer withstand the thermomechanical load and μ suddenly increases to a maximum value of 0.203. After reaching the maximum possible stroke of the loading mechanism of about 2 mm (peaks in Fig. 4, (a) and (c)), the wheel rotated for a while without further loading, and cooling continued until the end of the scheduled program time.

PVC-U is 2.5 times less thermally conductive than HDPE (0.2 and 0.5 W/m·K) [18], and Moss bamboo particles are more thermally conductive (k = 0.41-0.57 W/m·K) [19] compared to pine (k = 0.132 W/m·K) [20]. The temperature rise curve of composite material WPC-A is on average 10% higher than that of WPC-B up to a sliding distance of 2100 m. This could be explained by the fact that the heat generated in the contact zone of the friction pair passes through the much more conductive hard alloy plate faster than the less conductive composite material. The different glass transition T_g, melting T_m and crystallization T_c temperatures and structures of these composites determine their different behavior. Solid PVC is amorphous, although mechanically strong, but brittle, when reaching the glass transition temperature of around 80 °C, the mechanical properties become weaker, therefore reinforcing additives are used in production [21], while HDPE is semi-crystalline.

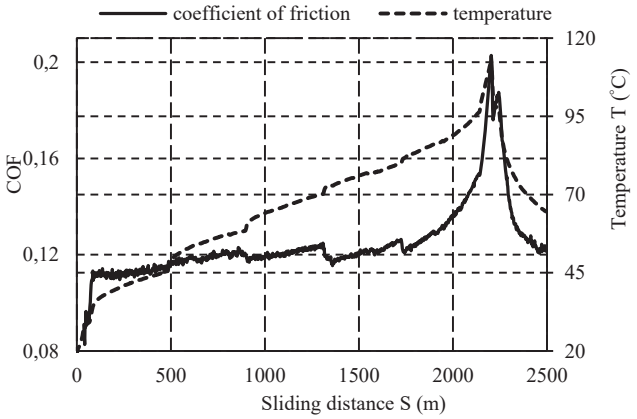

(a)

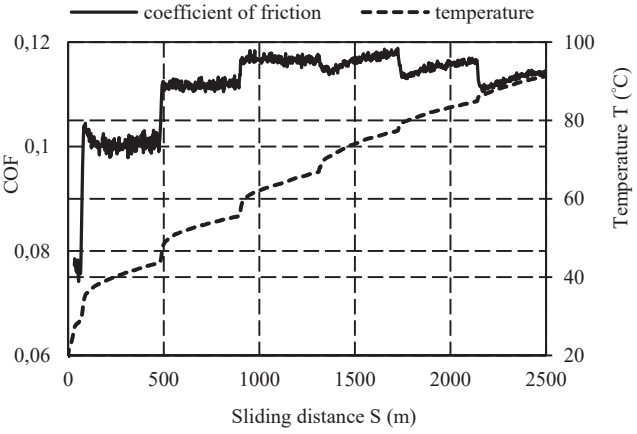

(b)

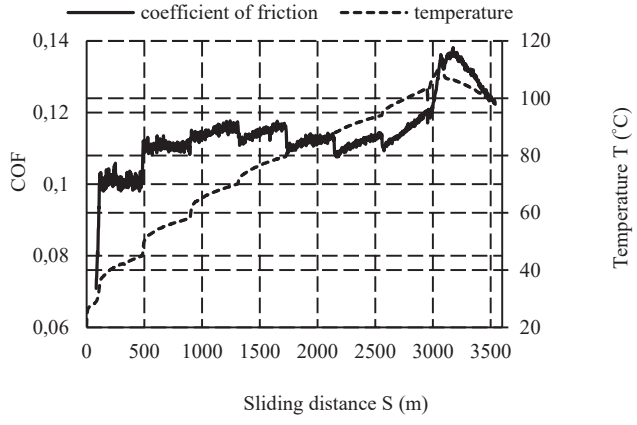

(c)

Fig. 6 Graphs of the evolution of the coefficient of friction: (a) WPC-A (F_{max} = 150.9 N, T_{max} = 111.8 °C, μ_{max} = 0.203); (b) WPC-B1 (F_{max} = 151.7 N, T_{max} = 91.3 °C, μ_{max} = 0.119); (c) WPC-B2 (F_{max} = 191.6 N, T_{max} = 111.8 °C, μ_{max} = 0.138)

Amorphous thermoplastics have better impact strength, but are more prone to stress cracking and have poorer fatigue

resistance than semi-crystalline thermoplastics [22]. Strong and wear-resistant HDPE thermoplastic is known to form an oriented transfer film in contact with metal, which lowers the coefficient of friction [23].

Firstly, a multiple regression analysis was performed to analyze only the effects of the S, F, and T factors with no interaction between them. In all cases, the adjusted coefficient of determination adj. R^2 close to 0.9 was obtained, indicating that a first-degree polynomial model explains 90% of the data scatter. Adj. $R^2 = 0.8986$ for composite WPC-A, and depending on the sign and size of the coefficient on the variable component, the temperature T (coefficient $\beta_3 = 2.899 \cdot 10^{-3}$) is the most important factor for increasing the coefficient of friction. Temperature is also the most important and positive factor ($\beta = 2.1546 \cdot 10^{-3}$) for WPC-B1 (adj. $R^2 = 0.8806$) and the most significant factor with the highest positive sign ($\beta = 1.552 \cdot 10^{-3}$), with a composite WPC-B2 (adj. $R^2 = 0.861$).

The interaction between the factors (SF, ST, FT, SFT) was then analyzed. Equations obtained according to (1) are presented in Table III.

TABLE III
REGRESSION DATA TABLE

Composite	Regression equation	Adj. R^2
WPC-A	$\mu = 2.6574 \cdot 10^{-2} - 3.6 \cdot 10^{-6}\,\mathbf{S} + 8.47 \cdot 10^{-4}\,\mathbf{F} + 1.902 \cdot 10^{-3}\,\mathbf{T} - 9.1 \cdot 10^{-7}\,\mathbf{SF} + 1.04 \cdot 10^{-7}\,\mathbf{ST} - 8.9574 \cdot 10^{-6}\,\mathbf{FT} + 7.5061 \cdot 10^{-9}\,\mathbf{SFT}$	0.9856
WPC-B1	$\mu = 1.225 \cdot 10^{-2} + 1.72 \cdot 10^{-3}\,\mathbf{F} + 1.134 \cdot 10^{-3}\,\mathbf{T} - 5.2 \cdot 10^{-7}\,\mathbf{SF} + 3.04 \cdot 10^{-7}\mathbf{ST} - 2.1 \cdot 10^{-5}\mathbf{FT} + 4.7 \cdot 10^{-9}\,\mathbf{SFT}$	0.9840
WPC-B2	$\mu = 1.8 \cdot 10^{-2} + 9.187 \cdot 10^{-4}\,\mathbf{F} + 2 \cdot 10^{-3}\,\mathbf{T} - 4.865 \cdot 10^{-7}\,\mathbf{SF} - 1.232 \cdot 10^{-5}\,\mathbf{FT} + 4.75 \cdot 10^{-9}\,\mathbf{SFT}$	0.9810

Table III shows that evaluating the interaction of factors, the adjusted R^2 of the WPC-A composite increased by approximately 8.8% to 0.9856. The magnitude and sign of the coefficient on the variable show that temperature was still the most significant factor, while force F was a positive but less significant factor. Since the sliding distance S was an insignificant factor alone for the WPC-B1 composite ($p = 0.577$), the recalculation was performed without it and the adjusted R^2 was increased by approximately 10% to 0.9840. The most significant factor is F, which is positive but less significant than T; the remaining factors are negative. The interaction between the sliding distance S and the factor pair ST was not significant in the composite WPC-B2 ($p > 0.7$), so after a recalculation without these members, the adj. R^2 rose about 12.3% to 0.981. The most significant factor was T.

The dependency of only the two most statistically significant factors (T and F) and the coefficient of friction μ = function (F, T) is shown in Fig. 7. The first-degree polynomial model based on (1) could only explain 72-84% of data scatter, therefore a second-degree polynomial (quadratic) model was chosen for a better fit of > 99%. As can be seen, the coefficient friction of WPC-A changes faster and in a wider range, the change is more pronounced when the glass transition temperature of the thermoplastic matrix is reached (phase shift) and the composite starts to soften and fracture.

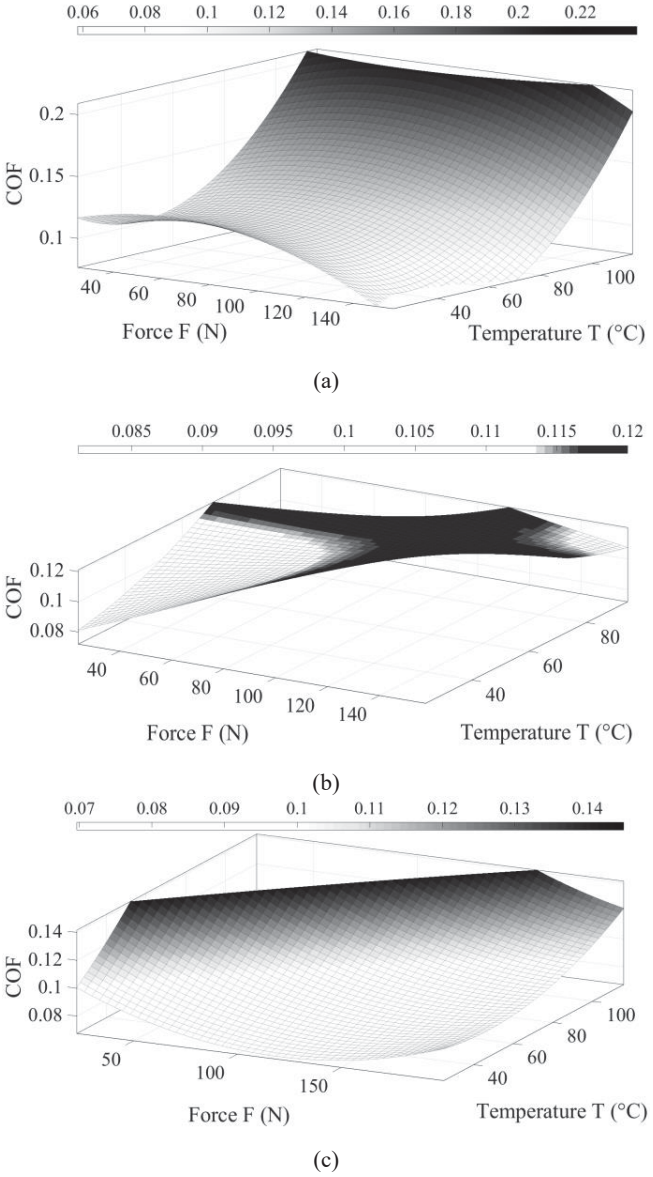

Fig. 7 Dependance of the COF on T and F variables: (a) WPC-A (adj. $R^2 = 0.9973$); (b) WPC-B1 (adj. $R^2 = 0.9968$); (c) WPC-B2 (adj. $R^2 = 0.9953$)

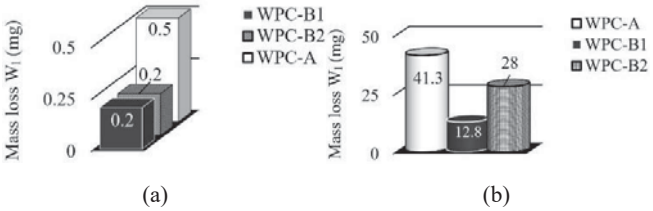

Fig. 8 The mass loss of friction pair elements: (a) hard alloy WC-Co plate; (b) WPC samples

The mass loss data are presented in Fig. 8. Since the wear is insignificant and the scale division value is 0.1 mg, the hard alloy material removal was estimated with an absolute error of ± 0.05 mg. The WC-Co, which worked in the friction pair with the WPC-A composite, had a mass reduction that was about 2.5

times greater. The same composite is less resistant to thermo-mechanical effects, has a higher coefficient of friction, and wears about 3.2 times faster than composite WPC-B1.

(a) (b) (c)

Fig. 9 View of the wheels after the test (a) WPC-A; (b) WPC-B1; (c) WPC-B2

(a)

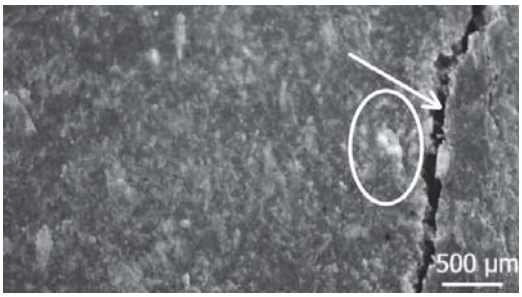

(b)

Fig. 10 DM images of the most deformed wheels after the test: (a) WPC-A; (b) WPC-B2; Oval symbol-wood particles, arrows-cracks

The image of the WPC samples after the test is shown in Fig. 9, and the digital microscope (DM) image of the most deformed wheels is shown in Fig. 10. The surface of the wheel WPC-A is worn, has cracks, the central part is most deformed, the surface is rough, a significant increase in width is visible (average width up to 5.5 and after the test 8.8 mm, Ø63.8 mm). Meanwhile, the wheel WPC-B1 is free of cracks and has a sufficiently smooth surface. After a longer test (51 min), the WPC-B2 wheel was also clearly plastically deformed, but in contrast to WPC-A, it deformed more laterally and began to break through the cracks that had formed at the edges and the wheel width increased significantly (up to ≈10 mm, Ø63 .8 mm).

C. SEM, Profile Roughness and EDS Test Results

SEM images and 20×20 µm segments of cemented carbide WC-Co surface wear (images processed with the Gwyddion 2.61 program) are presented in Fig. 11 in increasing order of wear severity (unworn, lightly worn and more heavily worn).

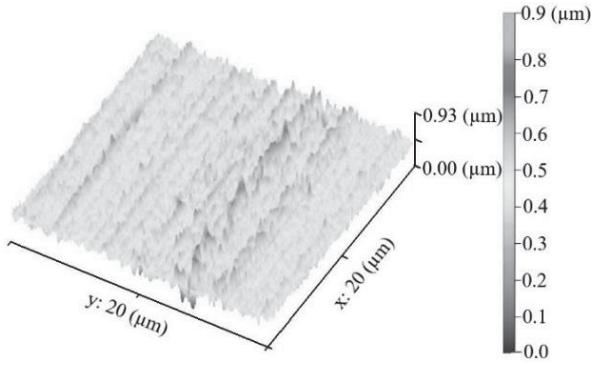

(a)

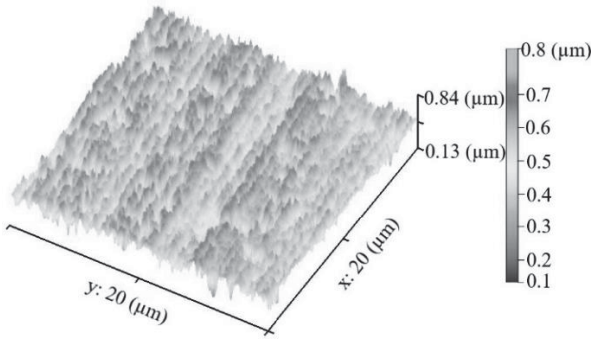

(b)

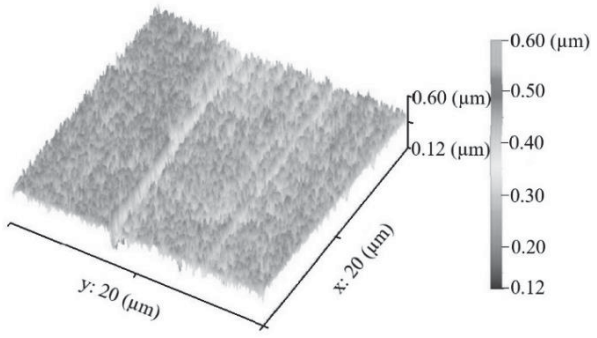

(c)

Fig. 11 WC-Co carbide surface image: (a) unworn; (b) WPC–B1 (lightly worn); (c) WPC–A (most worn)

The average roughness parameters of the cemented carbide surface profile are shown in Table IV. The mean is given with a 95% confidence interval according to (3).

The average Ra of carbide profile roughness is only slightly reduced for composite WPC-B1, while for composite WPC-A, the Ra value has decreased by about 3 times and the mean peak width Rsm has further increased by about 6.6. The maximum

profile peak height Rp has decreased by about 3 times and the root mean square slope Rdq has decreased by 4.5 times.

TABLE IV
PROFILE ROUGHNESS PARAMETERS

Parameter	BT[a]	±	AT[b]	±	Δ, %
			WPC-A		
Ra	0.094	0.017	0.078	0.003	-17%
Rsm	25.849	3.409	48.053	9.997	86%
Rp	0.228	0.076	0.183	0.042	-20%
Rdq	0.055	0.012	0.031	0.003	-45%
			WPC-B1		
Ra	0.109	0.010	0.102	0.004	-6%
Rsm	20.838	1.826	23.481	1.713	13%
Rp	0.267	0.043	0.251	0.024	-6%
Rdq	0.069	0.003	0.062	0.005	-10%

[a]BT-before the test; [b]AT-after the test.

TABLE V
EDS ELEMENTAL ANALYSIS RESULTS

	Elements	Before the test		After the test		Difference Δ
		Series	Nor. [wt. %]	Series	Nor. [wt. %]	Nor. [wt. %]
WPC-A	*W*	L	91.47	L	90.79	-0.74
	Co	K	2.98	K	3.74	+25.50
	C	K	2.77	K	2.58	-6.86
	O	K	0.37	K	0.15	-59.46
	Ni	K	1.13	K	1.66	+46.90
	Al	K	0.44	K	0.31	-29.55
	Cr	K	0.84	K	0.77	-8.33
	Total:		100		100	
WPC-B1	*W*	L	91.16	L	90.05	-1.22
	Co	K	3.16	K	3.00	-5.06
	C	K	2.47	K	3.64	+47.37
	O	K	0.36	K	1.07	+197.22
	Ni	K	1.25	K	1.24	-0.80
	Al	K	0.42	K	0.31	-26.19
	Cr	K	1.18	K	0.69	-41.53
	Total:		100		100	

The elemental composition results are shown in Table V. From the normalized weight results it can be seen, that the oxygen content on the surface of the WPC-A composite decreased more than several times after the test. It is well known that tungsten already starts to oxidize at room temperature [24], therefore the decrease in oxygen could be associated with changes in the oxide layer, oxidation reactions. Meanwhile, an increase in the amount of carbon and oxygen on the surface of the WPC-B1 composite is observed after the test. This could be related to the formation of a polymer composite transfer film on the hard alloy surface, which is dominated by the main polymer components of these elements.

IV. CONCLUSION

The dependence of the coefficient of friction on the three main factors (temperature, force and sliding distance) and their interactions in the dry friction pairs of the WPCs examined and the hard alloy WC-Co is explained by a polynomial model (adjusted coefficient of determination adj. $R^2 > 0.98$).

The maximum coefficient of friction of WPC-B composite was 32% lower compared to WPC-A. Composite WPC-B withstood about 30% higher load and longer sliding distance until the limit contact temperature was reached. Both the composite and the cemented carbide wore out the least.

REFERENCES

[1] K. Holmberg, A. Erdemir, "Influence of tribology on global energy consumption, costs and emissions", in *Friction* 5(3): 263-284 (2017), https://doi.org/10.1007/s40544-017-0183-5. Date of last access: 31.07.2023.

[2] D. M. Nuruzzaman, M. A. Chowdhury, "Friction and wear of polymer composites", Intechopen, 2012. DOI: 10.5772/48246.

[3] L. Deleanu, M. Botan, C. Georgescu, "Tribological behaviour of polymers and polymer composites", Intechopen, 2020. DOI: 10.5772/intechopen.94264.

[4] R. Johnson, "Wood plastic composites (WPC) market. Androit Market Research. Dallas, Texas, 2020", https://www.globenewswire.com. Date of last access: 20.09.2022.

[5] "Grand View Research. Wood plastic composites forecast 2022-2030", Report ID: 978-1-68038-849-7, p. 198. Date of last access: 22.09.2022.

[6] A. H. Elsheikh, H. Panchal, S. Shanmugan, T. Muthuramalingam, A. M. El-Kassas, B. Ramesh, "Recent progresses in wood – plastic composites: Pre - processing treatments, manufacturing techniques, recyclability and eco-friendly assessment", in *Cleaner Engineering and Technology*, Volume 8, June 2022, 100450, https://doi.org/10.1016/j.clet.2022.100450. Date of last access: 31.07.2023.

[7] D. J. Gardner, D. Murdock. "Extrusion of wood plastic composites", 2010, University of Maine, Orono, https://www.researchgate.net/publication/241788850_Extrusion_of_Wood_Plastic_Composites. Date of last access: 31.07.2023.

[8] C. Kneidinger, G. Zitzenbacher, "Friction between WPC bulk polymers and metal surfaces at high pressures and high velocity". *Conference: Symposium Polymermischungen 2011*. At: Halle an der Saale, Germany, Volume 14, https://www.researchgate.net/publication/. Date of last access: 21.07.2022.

[9] J. I. Orisaleye, S. J. Ojolo, "Parametric analysis and design of straight screw extruder for solid compaction", in *Journal of King Saud University* 31 (1): p. 86-96, DOI: 10.1016/j.jksues.2017.03.004. Project: Biomas Briquette Production, https://www.researchgate.net/publication/. Date of last access: 30.07.2023.

[10] W. Wu, C. He, Y. Qiang, H. Peng, M. Zhou, "Polymer – metal interfacial characteristics under ultrasonic plasticizing conditions: a united – atom molecular dynamic study", in *International Journal of Molecular Sciences*, 2022, 23, 2829, https://doi.org/10.3390/ijms23052829. Date of last access: 21.07.2022.

[11] "Extruder-KUHNE Maschinenbau", https://www.kuhne-mb.de/en/products/extruder. Date of last access: 21.07.2022.

[12] W. Wei, Y. Li, T. Xue, Y. Li, P. Sun, B. Yang, Z. Yin, and C. Mey, "Tool wear during high-speed milling of wood-plastic composites", in *Bio Resources*. 14(4), 8678-8688, 2019.

[13] Z. Zhu, D. Buck, J. Wang, Z. Wu, W. Xu, X. Guo, "Energy efficiency optimization for machining of wood plastic composite", in *Machines*, 2022, 10, 104. https://doi.org/10.3390/machines10020104. Date of last access: 21.07.2023.

[14] D. Saloni, U. Buehlmann, R. L. Lemaster, "Tool wear when cutting wood fiber-plastic composite materials", in *Forest Products Journal* (2011), 61 (2): 149-154.

[15] "2019-update 2021-Tigra. Tools cut better with TIGRA", https://www.tigra.com/media/pdf/47/7e/35/Woodworking-Catalog-2019.pdf. Date of last access: 21.07.2022.

[16] Y. C. Lin,Y. C. Chen, K. D. Wu, J. P. Hung, "Prediction of Surface Roughness based on the Machining Conditions with the Effect of Machining Stability", in *Advances in Science and Technology Research Journal*, Vol. 14, Issue 2, June 2020, p. 171-183. https://doi.org/10.12913/22998624/119048. Date of last access: 21.07.2023.

[17] S. H. Chen, C. H. Hsu, "Using uniform design and regression methodology of turning parameters study of nickel alloy", in *The International Journal of Advanced Manufacturing Technology* (2021) 116:3795-3808. Internet access: https://doi.org/10.1007/s00170-021-07584-4.

[18] "Material properties", https://material-properties.org/. Date of last access: 21.07.2023.
[19] D. U. Shah, J. Konnerth, M. H. Ramagel, C. Gusenbauer, "Mapping thermal conductivity across bamboo cell walls with scanning thermal microscopy", in *Scientific Reports*, (2019) 9:16667, https://doi.org/10.1038/s41598-019-53079-4. Date of last access: 21.07.2023.
[20] V. Çavuş, S. Şahin, B. Esteves, and U. Ayata, "Determination of thermal conductivity properties in some wood species obtained from Turkey", in *Bio Resources*, 2019, 14(3), 6709-6715.
[21] J. Tomaszewska, T. Sterzyński, A. W. Braszak, M. Banaszak, "Review of Recent Developments of Glass Transition in PVC Nanocomposites", in *Polymers (Basel)*, 2021 Dec; 13(24): 4336. DOI: 10.3390/polym13244336.
[22] B. Makreri, "The Difference Between Amorphous & Semi-crystalline Polymers", in *Impact plastics*, 2017, https://blog.impactplastics.co/blog/the-difference-between-amorphous-semi-crystalline-polymers. Date of last access: 21.07.2022
[23] I. Hutchings, "Tribology. Friction and wear of engineering materials", 2016, 2nd edition. ISBN: 978-0-08-100910-9.
[24] Y. Addab, C. Martin, C. Pardanaud, J. Khayadjian, K. Achkasov, "Formation of thin tungsten oxide layers: characterization and exposure to deuterium", in *Physica Scripta*, IOP Publishing, 2016. HAL ID: hal-03593478.